Co-published by
Institute of Fluid-Flow Machinery
Polish Academy of Sciences
Committee on Thermodynamics and Combustion
Polish Academy of Sciences

http://www.imp.gda.pl/archives-of-thermodynamics/

Online monitoring of thermal stress and heat transfer coefficient in thick-walled cylindrical elements

Jan Taler[a], Dawid Taler[a], Magdalena Jaremkiewicz[a*], Karol Kaczmarski[a], Tomasz Sobota[a], Krzysztof Smaza[b]

[a]Cracow University of Technology, Faculty of Environmental and Energy Engineering, ul. Warszawska 24, Cracow 31-155, Poland
[b]Evolution Group Krzysztof Smaza, ul. Sodowa 19/1, Cracow 30-376, Poland
*Corresponding author email: magdalena.jaremkiewicz@pk.edu.pl

Received: 30.07.2025; revised: 15.09.2025; accepted: 19.09.2025

Abstract

The article presents a method for online monitoring of thermal stress and heat transfer coefficient on the inner surface of a thick-walled cylindrical element using two separate applications. Both applications are based on the inverse heat conduction problem and use the control volume method. The first one allows the determination of thermal stresses based on measuring the wall temperature at a single point near the inner surface. This software is suitable for one-dimensional heat transfer, i.e. in a radial direction. The second application allows the heat transfer coefficient on the inner surface to be determined based on temperature measurements at six spatially distributed points. Knowledge of the heat transfer coefficient on the inner surface allows the stress concentration factor to be determined for elements weakened by an opening. This can be used to determine the optimum heating or cooling rates for pressure elements or to determine the thermal stresses in elements weakened by an opening. This method is suitable for heat transfer cases in the radial, longitudinal and circumferential directions. The correct operation of both original applications has been tested on a laboratory stand, where there was a sudden change in the working fluid temperature in a steam header from 16.8°C to 142.5°C. At the beginning of the temperature change, the thermal stresses on the header inner surface reached a maximum value of -195.8 MPa, and the heat transfer coefficient was approximately 5000 W/(m²K). Then, the thermal stresses began to decrease, and the heat transfer coefficient began to increase.

Keywords: Inverse heat conduction problem; Thermal stress; Heat transfer coefficient; C++ Builder; Visualisation

Vol. 46(2025), No. 3, 175–186; doi: 10.24425/ather.2025.156589

Cite this manuscript as: Taler, J., Taler, D., Jaremkiewicz, M., Kaczmarski, K., Sobota, T., & Smaza, K. (2025). Online monitoring of thermal stress and heat transfer coefficient in thick-walled cylindrical elements. *Archives of Thermodynamics*, 46(3), 175−186.

1. Introduction

Monitoring thermal stresses is essential in many industries, primarily in the energy sector (conventional, nuclear and renewable energy), but also in the metallurgical industry, semiconductor industry, automotive and aviation industries, transport, civil engineering and even medicine. The occurrence of excessive thermal stresses in structural components is one of the reasons for their failure due to material fatigue.

Non-destructive stress measurement methods include the magnetic property, strain gauge, and ultrasonic wave methods. However, these techniques are often problematic in the case of thermal stresses, although attempts are being made to adapt the measurement methods. For example, in [1], an improvement to the ultrasonic wave method was proposed by using piezoelectric zero-order shear horizontal (SH0) wave transducers bonded to the sample with adhesive. Work on this method was related to monitoring thermal stresses, which can cause cracking or bulging in railway rails.

The calculation method most commonly used in recent years for the analysis of thermal stresses is the finite element method (FEM).

Nomenclature

a – distance between nodes in the circumferential direction, m
A – surface area, m^2
b – distance between nodes in the longitudinal direction, m
c – specific heat capacity, J/(kg K)
E – Young's modulus, MPa
Fo – Fourier number
h – heat transfer coefficient, W/(m^2 K)
k – thermal conductivity, W/(m K)
p – pressure, MPa
$\dot{q}$ – heat flux, W/m^2
$\dot{q}_v$ – energy generation rate per unit volume, W/m^3
$\dot{Q}_{i,j}$ – heat flux rate transferred from node j to node i, W
r – radius or radial variable, m
s – thickness of the wall, m
t – time or time variable, s
T – temperature, K
$\bar{T}$ – mean temperature across wall thickness, K
v_T – rate of temperature change, K/s

Greek symbols

α – stress concentration factor
β – coefficient of linear thermal expansion, 1/K
δ – distance between the measuring point and the inner surface, m
Δr – spatial step in the radial direction, m
Δt – time step, s
ΔV – volume of the cell, m^3
$\Delta\varphi$ – spatial step in the circumferential direction, °
ε – tolerance, K
κ – thermal diffusivity, m^2/s
ν – Poisson's ratio
ρ – density, kg/m^3
σ – circumferential stress, MPa
ϕ – shape factor

Subscripts and Superscripts

al – allowable
b – spigot
direct– direct area
f – fluid
i – general node number index
in – inner
inv – inverse area
m – mean
out – outer
p – caused by pressure
P – on the edge of the hole at point P
s – shell
T – thermal

Abbreviations and Acronyms

FEM – finite element method
FVM – finite volume method
GUI – graphical user interface
IDE – integrated development environment
RAD – rapid application development
SH0 – zero-order shear horizontal (wave)
VCL – visual component library

The need to monitor thermal stresses in conventional power plants is related to the development of renewable energy. Renewable energy sources, primarily wind and solar energy, are unpredictable, necessitating more frequent start-ups and shutdowns of power units. This results in faster wear and tear due to fatigue of installation components, especially thick-walled components with complex shapes in steam boilers or steam turbines. Monitoring thermal stresses is also important because power plants often exceed their design life. Analysing the stresses that arise in the plant can help ensure safe operation and assess the residual strength of critical components. Finally, accurately determining thermal stresses makes it possible to determine the optimal start-up time [2] or shutdown time [3] for a conventional power plant. This time is determined based on the condition that the allowable stresses are not exceeded.

In energy installations, thick-walled components are used in high-pressure working fluid cases. In significant changes in fluid temperature, the greatest thermal stresses will occur on surfaces in contact with the fluid. The procedures for determining thermal stresses in these components are described in standards TRD 301 [4] and EN 12952-3 [5]. Monitoring thermal stresses using computational methods is strictly related to determining the temperature distribution in the analysed element and determining the heat transfer coefficient on the surface washed by the working fluid. If the component is not weakened by an opening, it is sufficient to know the temperature distribution in the wall. However, in practice, thick-walled elements have stubs that increase thermal stresses on the inner surface of the shell opening. Thermal stresses should then be calculated using the stress concentration factor, the value of which depends on the heat transfer coefficient.

Many studies on determining thermal stresses concern steam turbines [6–10]. In [6], a concept for an advanced turbine life monitoring system was proposed based on analysing damage caused by material fatigue. In [7], a modification of the algorithm based on Green's functions and the Duhamel integral was proposed, allowing the determination of thermal stresses in valves and turbine casings during start-up, considering the variable heat transfer coefficient. This method can be used for online stress monitoring. Online stress monitoring is also discussed in the article [8]. It presents a programme based on measurement data and calculations performed using FEM, which estimates stresses in critical turbine components (rotor, shut-off and control valves) and allows for optimisation of the device start-up. In [9], the thermal stresses occurring in the rotor of combined medium- and high-pressure turbines (with a common casing) were compared with the stresses in the rotors of turbines operating separately (in separate casings). In [10], thermal stresses occurring, among others, in a high-pressure steam turbine during start-up in the case of a deviation of the live steam temperature from that specified in the instructions were analysed.

Correct evaluation of thermal stresses is crucial in nuclear power plants, as it is related to the facility's safe operation. The main component of a pressurised water reactor is the pressure vessel, which must withstand the highest possible loads without any damage. Research on stresses and stress intensity factors in

reactor pressure vessel cracks was made in [11]. The work is based on the results of an experiment in which samples were exposed to thermal shock. Stress measurements were performed on samples with and without cracks using synchrotron X-ray diffraction as a function of time. At the same time, it was found that it is not possible to use FEM to simulate stresses during thermal shock under industrial conditions. The corners of the nozzles are critical points for pressure vessels in reactors. Research on methods for determining stresses in these areas, replacing the computationally expensive FEM method in this case, is presented, for example, in [12,13]. In [12], a simple method was developed for determining temperature distributions in the corner along the cross-section, taking into account heat conduction in two directions. Then, thermal stresses are calculated based on temperature gradients. In [13], on the other hand, it was proposed to determine the stress intensity factor based on simple predictive equations as a function of thermal load under cooling and heating conditions.

Thermal stresses naturally occur in other components of power plants where temperatures can change rapidly over time. For example, in [14], an analysis was performed of unsteady thermal stresses occurring in a safety condenser. The condenser is a shell-and-tube heat exchanger used in the event of an emergency shutdown of a steam turbine when hot steam needs to be cooled. The authors of the study used FEM to determine the temperature distribution in the shell and tubes of the condenser and assessed the thermal stresses during rapid start-up of the device. The calculations were performed for cases where a thermal expansion compensator was used in the condenser and without it.

The temperature field in a pressure element, knowledge of which allows thermal stresses to be determined, may result from a direct solution of the heat conduction problem. For example, [15] presents a method for predicting the behaviour of thick-walled elements with complex shapes, using the example of a Y-shaped junction, under unsteady conditions. The proposed method uses measurements obtained on the object with calculations performed using FEM. The paper also points to the significant influence of the heat transfer coefficient on the internal surface of the element on thermal stresses. Another example of determining the unsteady distribution of temperature and stresses in a cylindrical element using FEM is presented in [16]. The model developed for the calculations uses measurements of the ambient temperature, the external surface temperature and the temperature of the working fluid washing the internal surface. Also in [17], a cylindrical element was analysed using FEM for calculations. The model assumed that the pipeline was thermally insulated, and the temperature was measured using a new thermometer. The newly designed thermometer was used to obtain more accurate measurements of the working fluid temperature.

However, to solve the direct problem, it is necessary to know the internal surface temperature or the exact temperature of the working fluid and the heat transfer coefficient. In both cases, accurate measurements are difficult to achieve. Measuring the temperature of a fluid at high pressure and temperature requires the use of thermometers in heavy housings, which causes a significant dynamic measurement error. Another approach to calculating the temperature distribution in a pressure element, which then allows the determination of thermal stresses, is to solve the inverse heat conduction problem [18]. In this case, it is sufficient to know the temperature at one or more points inside the wall of the element. Examples of articles in which this method is developed are [19−22]. In [19], the temperature distribution in a thermally insulated cylindrical wall is determined based on the measurement of the external surface temperature, and in [20,21] based on the measurement of the temperature near the internal surface. In these cases, heat was assumed to be transferred only in the radial direction. In [22], on the other hand, the inverse problem is solved by measuring the wall temperature at six points, which allows the internal surface temperature and the heat transfer coefficient to be determined for a three-dimensional temperature distribution. The inverse methods can also be used to assess the influence of wall material heterogeneity on temperature distribution and stress. For example, in [23], the temperature distribution and thermal stresses in a spherical, hollow element made of functionally graded material were analysed based on the known temperature and circumferential strain on the outer surface. The problem was reduced to an inverse thermoelasticity problem and solved using FEM.

In inverse methods, the problems of direct methods are eliminated, but they are sensitive to random errors in the measurement data used as input. The impact of random errors can be reduced by using regularisation methods, such as the Tikhonova method and its modifications [24,25] or the method based on the notation of the thermal balance [26]. Random errors can also be eliminated by smoothing the measurement data using digital filters [27], which is a simple and effective solution.

This article presents simple and effective methods for monitoring thermal stresses in an element without an opening and determining the heat transfer coefficient on the inner surface of a pressure element in unsteady states. Both methods apply to thick-walled cylindrical elements and are based on solving the inverse heat conduction problem. The first method is based on measuring the temperature inside the element wall at a single point and is suitable for heat conduction in the radial direction. Thermal stresses are determined based on the standard [5]. The second method is based on measuring the temperature at six points inside the wall of the element. It is suitable for heat transfer in three directions (longitudinal, circumferential and radial). The operation of both applications has been verified on a laboratory stand equipped with a thick-walled steam header.

2. Determination of circumferential stress in thick-walled cylindrical elements

Pressure components exposed to variable loads, e.g. due to cyclic start-up and shutdown of units, should be subjected to fatigue analysis. Operating and environmental influences that cause variable loads include, among others, changing pressure and temperature of the working fluid, unsteady temperature conditions, restrictions on expansion or contraction of the material during normal temperature changes, forced vibrations, or changing external loads. Circumferential stresses in cylindrical elements should meet condition [5]:

$$\sigma \le \sigma_{al}. \tag{1}$$

The allowable stresses σ_{al} for the designed number of cycles are determined for a given material and specific tensile strength R_m using, for example, the Wohler diagram [5].

If the circumferential stresses are caused only by changes in the pressure and temperature of the working medium, the maximum circumferential stresses on the inner surface of the hole at point P (Fig. 1) can be determined using the equation [5]:

$$\sigma_{\mathrm{P}} = \alpha_p \sigma_p + \alpha_T \sigma_T. \tag{2}$$

Figure 1 shows a section of a thick-walled pipe with thermal stress and stress caused by pressure at point P on the inner surface of the hole marked.

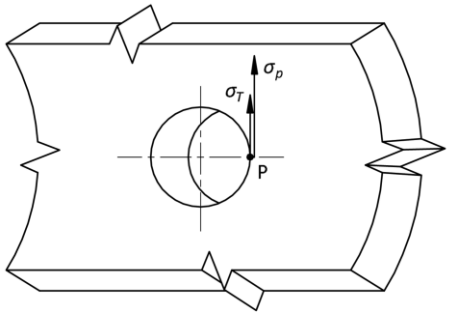

Fig. 1. View of a fragment of a thick-walled element weakened by a hole with marked circumferential stresses at point P on the edge of the hole.

Circumferential stresses caused by pressure are calculated using the following equation:

$$\sigma_p = \frac{p r_{ms}}{s}. \tag{3}$$

The mean radius of a cylindrical element r_m is calculated as the arithmetic mean of the inner r_{in} and outer r_{out} radii.

Thermal stresses reach their highest values on the inner surface and are determined using the formula:

$$\sigma_T = \frac{E\beta}{1-\nu}\left(\bar{T} - T|_{r=r_{in}}\right). \tag{4}$$

The mean temperature function across the cylindrical wall thickness $\bar{T}$ in Eq. (4) is determined by the following equation:

$$\bar{T} = \frac{2}{r_{out}^2 - r_{in}^2}\int_{r_{in}}^{r_{out}} rT(r,t)dr. \tag{5}$$

Standard [5] presents a procedure for calculating thermal stresses for a quasi-steady state when the temperature of the pipeline wall changes over time at a constant rate and the pipeline is thermally insulated. The formula contained in standard [5] is derived from the solution of the heat conduction equation, which for isotropic bodies has the general form [28]:

$$c(T)\rho(T)\frac{\partial T}{\partial t} = \nabla \cdot [k(T)\nabla T] + \dot{q}_v, \tag{6}$$

and which for heat transfer in the radial direction, constant pipeline material properties and zero energy generation per unit volume has the form:

$$\frac{1}{r}\frac{d}{dr}\left(r\frac{dT}{dr}\right) = \frac{v_T}{\kappa}. \tag{7}$$

From solving Eq. (7) with boundary conditions:

$$T|_{r=r_{in}} = v_T t, \tag{8}$$

$$-k\frac{dT}{dr}\Big|_{r=r_{out}} = 0, \tag{9}$$

we obtain:

$$T = v_T t + \frac{1}{4}\frac{v_T}{\kappa}\left(r^2 - r_{in}^2 - 2r_{out}^2 \ln\frac{r}{r_{in}}\right). \tag{10}$$

After substituting Eq. (10) into Eqs. (5) and (4), we obtain:

$$\sigma_T = \phi\frac{E\beta}{1-\nu}\frac{v_T s^2}{\kappa}, \tag{11}$$

where

$$\phi = \frac{1}{8}\frac{(u^2-1)(3u^2-1)-4u^4\ln u}{(u^2-1)(u-1)^2}, \tag{12}$$

and $u = r_{out} / r_{in}$.

For an unsteady state, the integral in Eq. (5) can be calculated using, for example, the trapezoidal method. This requires calculating the temperature T_i at N equidistant discrete points (at a distance Δr) on the radii r_i:

$$\bar{T} = \frac{1}{r_{out}^2 - r_{in}^2}\sum_{i=2}^{N}(r_{i-1}T_{i-1} + r_i T_i)\Delta r. \tag{13}$$

The temperature at N points can be obtained using numerical methods, e.g. the finite volume method (FVM) or finite element method (FEM).

The stress concentration factor due to pressure is determined by Eq. [5]:

$$\alpha_p = 2.2 + e^{A}\zeta^{B}, \tag{14}$$

where

$$A = -1.14\left(\frac{s_b}{s_s}\right)^2 - 0.89\frac{s_b}{s_s} + 1.43, \tag{15}$$

$$B = 0.326\left(\frac{s_b}{s_s}\right)^2 - 0.59\frac{s_b}{s_s} + 1.08, \tag{16}$$

$$\zeta = \frac{r_{mb}}{r_{ms}}\sqrt{\frac{r_{ms}}{s_s}}. \tag{17}$$

The thermal stress concentration factor is calculated as follows [5]:

$$\alpha_T = \left\{\left[2 - \frac{h+2700}{h+1700}z + \frac{h}{h+1700}(e^{-7z} - 1)\right]^2 + 0.81z^2\right\}^{\frac{1}{2}}, \tag{18}$$

where $z = r_{mb} / r_{ms}$.

Standard [5] proposes to adopt constant values for the heat transfer coefficient h: 3000 W/(m^2 K) for water and 1000 W/(m^2 K) for steam. Determining the exact value of the heat transfer coefficient, especially in the case of significant deviations from the value given in the standard, increases the accuracy of thermal stress calculations.

3. Method for determining a one-dimensional temperature field by measuring the temperature at a single point on the wall

The one-dimensional temperature field in the wall of a cylindrical element, knowledge of which is necessary to determine the mean wall temperature from Eq. (13) and thermal stresses from Eq. (4), can be determined using the inverse method. The proposed method uses a wall temperature measurement at a single point and the fact that the pipeline is thermally insulated. The temperature measurement point N divides the cross-sectional area of the pipe into a direct ($r_N \le r \le r_{out}$) and inverse ($r_{in} \le r \le r_N$) area (Fig. 2).

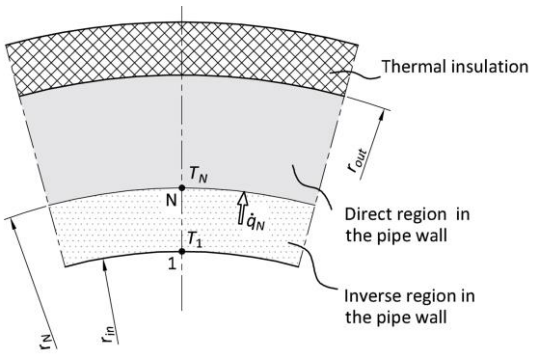

Fig. 2. Cross-section of the pipe with a marked temperature measurement point N and division into inverse ($r_{in} \le r \le r_N$) and direct ($r_N \le r \le r_{out}$) areas.

To determine the temperature field, the heat conduction Eq. (6) was used, which for heat transferred in the radial direction, the lack of energy generation rate per unit volume and the temperature-dependent physical properties of the pipeline material takes the form [20,27]

$$c(T)\rho(T)\frac{\partial T}{\partial t} = \frac{1}{r}\frac{\partial}{\partial r}\left[k(T)r\frac{\partial T}{\partial r}\right]. \tag{19}$$

The equation is first solved for the direct area and boundary conditions

$$T|_{r=r_N} = T_N, \tag{20}$$

$$-k(T)\frac{\partial T}{\partial r}\Big|_{r=r_{out}} = 0. \tag{21}$$

From the solution of the direct problem, Eqs. (19)–(21), we obtain the temperature distribution over the wall thickness in the direct region and the heat flux at point N. Thus, the second boundary condition on the isothermal surface on which point *N* is located is known and has the form of Eq. (23). The boundary conditions for solving the inverse problem are as follows:

$$T|_{r=r_N} = T_N, \tag{22}$$

$$-k(T)\frac{\partial T}{\partial r}\Big|_{r=r_N} = \dot{q}_N. \tag{23}$$

From the solution of the obtained inverse problem, Eqs. (19) and (22)–(23), we get the temperature distribution over the wall thickness in the inverse region, including the temperature at the inner surface of the pipeline.

3.1. Solution of the inverse problem

FVM will be used to solve the inverse problem. The heat balance equation for a single control volume, which is obtained by transforming Eq. (6), is of the form [28]:

$$\Delta V_i c(T_i)\rho(T_i)\frac{\partial T_i}{\partial t} = \sum_{j=1}^{n_c}\dot{Q}_{i,j} + \Delta V_i \dot{q}_v(T_i). \tag{24}$$

The inverse area in the proposed algorithm was divided into two control volumes, as shown in Fig. 3. The division of the inverse area into only two finite volumes was dictated by the small distance of the temperature measuring point from the inner surface. If the measuring point is at a greater distance from the inner surface, the algorithm can be modified, and the number of control volumes can be increased.

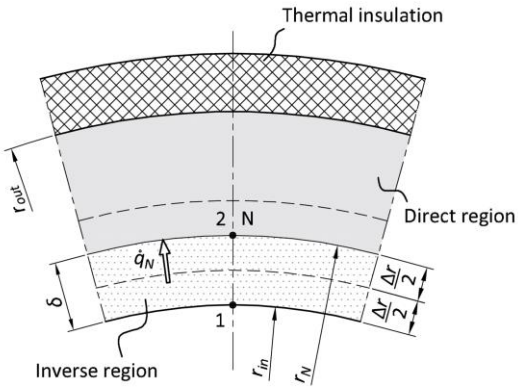

Fig. 3. Division of the inverse region into two finite volumes.

In this case, the internal surface temperature (at node 1) T_1 is determined from the energy balance equation for node 2, which coincides with the temperature measurement point N. In the case under consideration, the energy generation rate per unit volume equals zero.

The energy balance for node 2 has the form:

$$\pi\left[{r_N}^2 - \left(r_N - \frac{\Delta r}{2}\right)^2\right]c(T_N)\rho(T_N)\frac{dT_N}{dt} = \\ = 2\pi\left(r_N - \frac{\Delta r}{2}\right)\frac{k(T_1)+k(T_N)}{2}\frac{T_1 - T_N}{\Delta r} + 2\pi r_N \dot{q}_N. \tag{25}$$

Hence, the temperature at the inner surface is:

$$T_1 = \frac{(\Delta r)^2\left(r_N - \frac{\Delta r}{4}\right)}{r_N - \frac{\Delta r}{2}}\frac{c(T_N)\rho(T_N)}{k(T_1)+k(T_N)}\frac{dT_N}{dt} - \frac{2r_N\Delta r}{r_N - \frac{\Delta r}{2}}\frac{\dot{q}_N}{k(T_1)+k(T_N)} + T_N. \tag{26}$$

In Eq. (26), there is a thermal conductivity coefficient $k(T_1)$, which is calculated from the temperature at node 1. Iterative calculations are therefore necessary, with the first iteration assuming that the temperature at node 1 is equal to the temperature at node 2 (at point N). Iterations are carried out until the condition is met:

$$\left|T_1^{(n+1)} - T_1^{(n)}\right| \le \varepsilon, \tag{27}$$

where the tolerance $\varepsilon \approx 0.00001$ K.

The calculation algorithm is as follows. For a given time t, based on the temperature T_N measured at point N and smoothed with a digital filter, the temperature distribution in the direct region and the heat flux $\dot{q}_N$ are determined from the solution of the direct problem. Then, from $\dot{q}_N$ and temperature T_N, the temperature at node 1 is calculated from Eq. (26). From the solution of the direct and inverse problem, the mean temperatures for the two areas $\bar{T}_{direct}$ and $\bar{T}_{inv}$ are determined separately.

From these and based on the transformed Eq. (5), the mean temperature over the wall thickness is determined:

$$\bar{T} = \frac{2}{r_{out}^2 - r_{in}^2}\int_{r_{in}}^{r_{out}} rT(r,t)dr = \\ = \frac{2}{r_{out}^2 - r_{in}^2}\left[\int_{r_{in}}^{r_N} rT(r,t)dr + \int_{r_N}^{r_{out}} rT(r,t)dr\right] = \\ = \frac{2}{r_{out}^2 - r_{in}^2}\left(\frac{r_N^2 - r_{in}^2}{2}\bar{T}_{inv} + \frac{r_{out}^2 - r_N^2}{2}\bar{T}_{direct}\right). \quad (28)$$

Finally, the stress due to pressure from Eq. (3) and the thermal stress from Eq. (4) are calculated. The whole algorithm is then repeated for time $t + \Delta t$.

For the solution of the inverse problem to be stable, the time step must be chosen appropriately. In this respect, the condition must be met:

$$\mathrm{Fo} \geq 0.05, \quad (29)$$

where

$$\Delta\mathrm{Fo} = \frac{\kappa \Delta t}{(r_N - r_{in})^2}. \quad (30)$$

4. Method for determining the heat transfer coefficient based on temperature measurements at six points

The heat transfer coefficient at the inner surface of the pipeline can be determined using FVM. The proposed method is suitable for cases where the temperature field in the wall of a thick-walled element is unsteady and is a function of radial, circumferential and longitudinal variables, the element has a complex shape, as well as when the use of correlations on the Nusselt number is difficult to implement. Correlations on the Nusselt number are usually created for cases of hydraulically developed fluid flow, and this condition is not always achieved at a given point in the pipeline due to different types of fittings (elbows, branches, reducers, etc.) or other equipment (valves, etc.). The method is based on measuring the wall temperature at six points: C, U, N. S, W and E near the inner surface of the pipeline (Fig. 4). The measurement of the temperature at the six points and the subdivision into control volumes as shown in Fig. 4 is based on the assumption that heat in a cylindrical wall is transferred in the radial, circumferential and longitudinal directions. From the temperature measurements, the temperature at the inner surface of the pipeline at point L is calculated. The nodes C, U, N, S, W and E lie at the centres of gravity of the control volumes, whose thickness is Δr. The control volume with node L has a thickness of $\Delta r/2$, and node L lies on the inner surface of the pipe.

Nodes C, N, S, W and E are located at a distance $\delta_1 = \Delta r$ and node U at a distance $\delta_2 = 2\Delta r$ from the inner surface. Nodes N and S are located at a distance a in the circumferential direction, above and below the central node C, respectively. Nodes E and W are located at a distance b in the longitudinal direction, to the left and right of node C, respectively. Node U and L are located at a distance Δr in the radial direction, behind and in front of C, respectively.

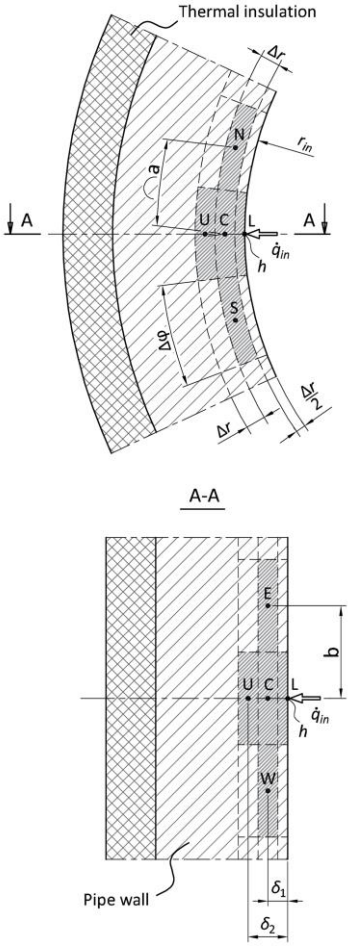

Fig. 4. Division of a pipeline section into control volumes.

The temperature at the internal surface is calculated from the energy balance for the control volume with node C, determined using Eq. (24). Assuming the material properties of the pipeline as a function of temperature, it can be written that:

$$\Delta V_C c(T_C)\rho(T_C)\frac{dT_C}{dt} = \frac{A_{U-C}}{\Delta r}\frac{k(T_U)+k(T_C)}{2}(T_U - T_C) + \\ + \frac{A_{L-C}}{\Delta r}\frac{k(T_L)+k(T_C)}{2}(T_L - T_C) + \frac{A_{N-C}}{a}\frac{k(T_N)+k(T_C)}{2}(T_N - T_C) + \\ + \frac{A_{S-C}}{a}\frac{k(T_S)+k(T_C)}{2}(T_S - T_C) + \frac{A_{W-C}}{b}\frac{k(T_W)+k(T_C)}{2}(T_W - T_C) + \\ + \frac{A_{E-C}}{b}\frac{k(T_E)+k(T_C)}{2}(T_E - T_C), \quad (31)$$

where

$$\Delta V_C = \frac{\Delta\varphi}{2\pi}\pi\left[\left(r_{in} + \frac{3}{2}\Delta r\right)^2 - \left(r_{in} + \frac{1}{2}\Delta r\right)^2\right]b, \quad (32)$$

$$A_{U-C} = \frac{\Delta\varphi}{2\pi}2\pi\left(r_{in} + \frac{3}{2}\Delta r\right)b, \quad (33)$$

$$A_{L-C} = \frac{\Delta\varphi}{2\pi}2\pi\left(r_{in} + \frac{1}{2}\Delta r\right)b, \quad (34)$$

$$A_{\mathrm{N-C}} = A_{\mathrm{S-C}} = \Delta r b, \tag{35}$$

$$A_{\mathrm{W-C}} = A_{\mathrm{E-C}} = \frac{\Delta\varphi}{2\pi}\pi\left[\left(r_{in}+\frac{3}{2}\Delta r\right)^2 - \left(r_{in}+\frac{1}{2}\Delta r\right)^2\right]. \tag{36}$$

The internal surface temperature at node L derived from Eq. (31) is of the form

$$\begin{aligned} T_{\mathrm{L}} = {} & 2\Delta r \frac{c(T_{\mathrm{C}})\rho(T_{\mathrm{C}})}{k(T_{\mathrm{L}})+k(T_{\mathrm{C}})}\frac{\Delta V_{\mathrm{C}}}{A_{\mathrm{L-C}}}\frac{dT_{\mathrm{C}}}{dt} - \frac{A_{\mathrm{U-C}}}{A_{\mathrm{L-C}}}\frac{k(T_{\mathrm{U}})+k(T_{\mathrm{C}})}{k(T_{\mathrm{L}})+k(T_{\mathrm{C}})}(T_{\mathrm{U}}-T_{\mathrm{C}}) + \\ & - \frac{A_{\mathrm{N-C}}}{A_{\mathrm{L-C}}}\frac{\Delta r}{a}\frac{k(T_{\mathrm{N}})+k(T_{\mathrm{C}})}{k(T_{\mathrm{L}})+k(T_{\mathrm{C}})}(T_{\mathrm{N}}-T_{\mathrm{C}}) + \\ & - \frac{A_{\mathrm{S-C}}}{A_{\mathrm{L-C}}}\frac{\Delta r}{a}\frac{k(T_{\mathrm{S}})+k(T_{\mathrm{C}})}{k(T_{\mathrm{L}})+k(T_{\mathrm{C}})}(T_{\mathrm{S}}-T_{\mathrm{C}}) + \\ & - \frac{A_{\mathrm{W-C}}}{A_{\mathrm{L-C}}}\frac{\Delta r}{b}\frac{k(T_{\mathrm{W}})+k(T_{\mathrm{C}})}{k(T_{\mathrm{L}})+k(T_{\mathrm{C}})}(T_{\mathrm{W}}-T_{\mathrm{C}}) + \\ & - \frac{A_{\mathrm{E-C}}}{A_{\mathrm{L-C}}}\frac{\Delta r}{b}\frac{k(T_{\mathrm{E}})+k(T_{\mathrm{C}})}{k(T_{\mathrm{L}})+k(T_{\mathrm{C}})}(T_{\mathrm{E}}-T_{\mathrm{C}}) + T_{\mathrm{C}}. \end{aligned} \tag{37}$$

Then, knowing the temperatures at nodes U, C and L allows the heat flux at node L to be calculated from Eq. (29):

$$\dot{q}_{\mathrm{L}} = -k(T_{\mathrm{L}})\frac{-3T_{\mathrm{L}}+4T_{\mathrm{C}}-T_{\mathrm{U}}}{2\Delta r}. \tag{38}$$

The calculated heat flux and temperature at the L node on the internal surface and the measured temperature of the working fluid T_f allow the heat transfer coefficient to be determined:

$$h_{\mathrm{L}} = \frac{\dot{q}_{\mathrm{L}}}{T_f - T_L}. \tag{39}$$

In Eq. (37), knowledge of the thermal conductivity coefficient $k(T_{\mathrm{L}})$ is needed, so iterative calculations must be carried out to calculate the temperature T_{L}. In the first iteration, the temperature at node L is assumed to be equal to the temperature at node C. Iterations are carried out until the condition is satisfied:

$$\left|T_{\mathrm{L}}^{(n+1)} - T_{\mathrm{L}}^{(n)}\right| \le \varepsilon, \tag{40}$$

where the tolerance $\varepsilon \approx 0.00001$ K.

In the calculation algorithm, first the measured data, i.e. temperatures T_{U}, T_{C}, T_{S}, T_{E} and T_{W} for time t are smoothed using a digital filter. Then the temperature T_{L} from Eq. (37) is determined in an iterative calculation. In subsequent steps, the heat flux $\dot{q}_{\mathrm{L}}$ from Eq. (38) and the heat transfer coefficient h_{L} from Eq. (39) are calculated. The entire algorithm is then repeated for the next time $t + \Delta t$.

5. Laboratory bench description

The test bench, on which the new temperature measuring sensors were installed, is shown in Fig. 5. The measurements taken with the thermometers are the input data for the developed applications. The main component of the bench is a Viessmann VITOMAX 200 HS (type M237) oil-fired steam generator with a thermal output of 460 kW and a steam output of 700 kg/h (saturated steam at 10 bar). In addition, the station includes a feedwater treatment station, deaerator, sludge expander, 10/4/2 bar reduction station and steam header.

The experimental tests were carried out while the system was in operation. During boiler start-up, the steam header was taken out of the circuit. When the oil-fired boiler reached its nominal heat output, a valve on the inlet pipe to the header was slowly opened, allowing steam to flow. The boiler produces saturated steam, but because a throttle orifice was fitted upstream of the header, superheated steam flows through it.

Fig. 5. General view of the laboratory station: 1 - steam boiler, 2 - deaerator, 3 - sludge expander, 4 - water treatment station, 5 - reduction station, 6 - steam header.

The temperature measuring sensors were mounted in a thick-walled steam header. The steam header was made from P91 martensitic steel. It is a thick-walled pipe with a length of 3.765 m, an outside diameter of 0.355 m and a wall thickness of 0.05 m. Three sheathed thermocouples were installed in the header to measure the steam temperature. These thermometers have different outer jacket diameters: 1, 2 and 3 mm. To ensure that the 1 and 2 mm diameter thermometers are not damaged or bent as the steam flows through the header, they are contained in sheath tubes for almost their entire length inside the header. The thermometer used to measure the wall temperature at one point near the inner surface is a sheathed thermocouple with an outer diameter of 3 mm. It is placed in a drilled hole 42.5 mm deep; thus, the tip of the thermometer is at a distance of δ = 7.5 mm from the inner surface of the header. A measuring probe consisting of five rod-shaped elements with diameters of 10 mm was used to measure the temperature of the steam header wall at six points. One of the rods has four grooves milled longitudinally, spaced every 90° with respect to the cross-section. In two of the opposite grooves, thermocouples have been placed so that their tips are at the end of the rod, while in the other two, the measuring junctions are at a distance of 7.5 mm from the end of the rod. This is the central rod placed in a 42.5 mm deep hole inside the wall, halfway up the header. Each of the other four rods has two grooves milled longitudinally on opposite sides, in which the thermocouples are placed so that their ends are at the end of the rod. These rods are also placed in holes 42.5 mm deep. Relative to the end of the central rod, their ends are located at a distance of 50 mm, below and above in the circumferential direction and to the left and right in the longitudinal direction. The measuring probe elements mounted in this way allow the wall temperature to be measured at 5 points at a distance of δ_1 = 7.5 mm from the inner surface and at 1 point at δ_2 = 15 mm from the inner surface.

The thermocouples in the measuring probe have a sheath diameter of 1.5 mm. The temperature at the subsequent measuring points is the arithmetic average of each pair of thermocouples. All thermocouples used, i.e. for measuring the temperature of the steam and the temperature of the header wall at one point and in the measuring probe, are of type K, class 2, with a grounded measuring junction. Before installation, they were calibrated using a calibration furnace. For wall temperature measurements, thermally conductive paste has been applied inside the holes before the insertion of the thermometer or measuring probe rods to minimise contact resistance. The installation of the measuring sensors is shown in Figs. 6 and 7.

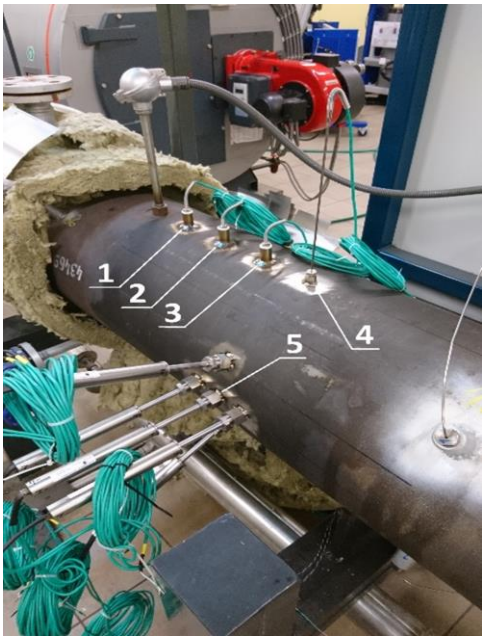

Fig. 6. The way of assembling the temperature measuring sensors: 1−3 - steam temperature measurement by thermocouples with outer jacket diameters of 1, 2 and 3 mm; 4 - pipeline wall temperature measurement at one point, 5 - measuring probe (pipeline wall temperature measurement at 6 points).

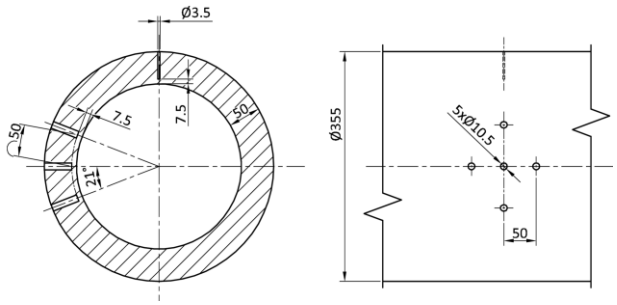

Fig. 7. Method of making holes for sensors to measure the temperature of the steam header wall.

The choice of location of the temperature measurement sensors in the wall of the steam header was due to how the temperature field in the wall changes in different parts of it. During the experiment, the steam flowing into the cold, thick-walled pipe partially condenses on its inner surface. This results in a lower wall temperature near the bottom of the header, where the condensate collects, than in the upper part. This is confirmed by temperature measurements around the circumference of the pipe. These measurements indicate that in the pipe's upper part, the temperature field is one-dimensional (heat is transferred only in the radial direction). Hence, it follows that the measurement of the element wall temperature at one point is carried out at the top of the steam manifold. Using a measuring probe that allows the wall temperature to be measured at 6 points is justified if there is at least a two-dimensional temperature field obtained in the lower part of the steam header. Hence, the probe's location, i.e. halfway up the pipe, results.

During the tests, in addition to temperature measurements, the pressure at the outlet of the header and the mass flux of the steam were also measured. Pressure is measured using a pressure gauge with a U-tube syphon and a cock. The pressure gauge is class 1 and has a measuring range of 16 bar, which means an accuracy of ±0.16 bar. The steam flow rate is measured using an orifice plate with a measurement accuracy of ±1.5% of the measured value.

The measurements are recorded by the data acquisition system every $\Delta t = 1$ s.

Measurements performed on the bench are recorded on a continuous basis using Metronic's M-800 analogue signal transmitters with an RS-485 serial communication port. The transmitter has a built-in Modbus RTU protocol for reading current results, controlling output relays, and transferring data to a computer. Astor Sp. z o.o.'s. InTouch software was used to visualise and control the processes occurring throughout the system. It enables the observation of processes taking place in the installation and its parts presented as graphic objects on the monitor screen. It also allows the measured parameters to be presented in graphical form. A fragment of a graphic visualisation of a pipe section, on which temperature measurements using the described sensors are conducted, is presented in Fig. 8 (the screenshot was taken when the installation was not in operation).

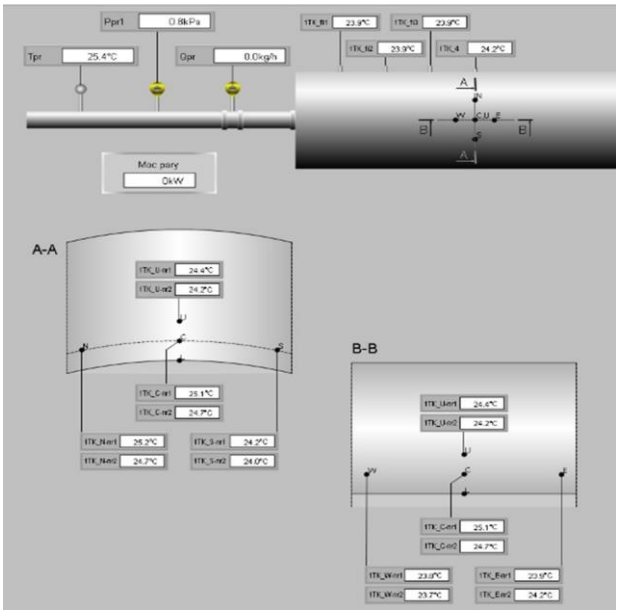

Fig. 8. Fragment of a screen shot from the visualisation software of measurements carried out on a thick-walled steam header (during system shutdown).

6. Description of the software and its test on the laboratory bench

Two applications were developed based on the computational algorithms described in Sections 2−4: 'Thermal Stress Monitoring' and 'Identification of Heat Transfer Coefficient'. The 'Thermal Stress Monitoring' application allows the determination of thermal stresses and stresses due to the pressure of the working fluid on the inner surface based on temperature measurements at a single point inside the wall of the steam collector. In the application, stresses caused by pressure are calculated using Eq. (3), while thermal stresses on the inner surface are determined using Eq. (4). The mean temperature across the pipe wall thickness and the inner surface temperature, which are necessary for calculating thermal stresses, are determined using Eqs. (28) and (26), respectively. In turn, the 'Identification of Heat Transfer Coefficient' application calculates the heat transfer coefficient on the inner surface of the steam header based on temperature measurements at six points inside the pipe wall. Based on these values, the internal pipe surface temperature is determined from Eq. (37) and the heat flux from Eq. (38). Next, the heat transfer coefficient is calculated from Eq. (39).

Both software programs use the following properties of the steam header steel for their calculations:

$$k(T) = -0.003 \times 10^{-10}T^5 + 4.741 \times 10^{-10}T^4 + \\ -2.874 \times 10^{-7}T^3 + 6.438 \times 10^{-5}T^2 + \\ -4.177 \times 10^{-4}T + 28.676, \quad (41)$$

$$c(T) = 1.41 \times 10^{-6}T^3 - 6.43 \times 10^{-4}T^2 + \\ +4.88 \times 10^{-1}T + 439.80, \quad (42)$$

and density ρ = 7750 kg/m^3. The density value was taken constant due to the fact that it varies little for the expected temperature range of the header wall. The properties of the steel were taken from [5].

As the inverse methods used in the applications are sensitive to random measurement errors, the temperature measurements were smoothed using a 9-point digital filter [29].

Both applications were written in the Embarcadero C++ Builder 12 environment. C++ Builder is an Integrated Development Environment (IDE), which is distinguished by the fact that it allows the rapid development of Rapid Application Development (RAD) applications thanks to an extensive palette of Graphical User Interface (GUI) components. The used C++ programming language with Embarcadero extensions enabled visual programming. The compiler is based on Clang for Win64 compatible with C++ version 17. The environment includes a wide range of pre-built components such as buttons, text boxes, drop-down lists, tables, grids, database components, charts, etc. The applications use a graphical interface based on the Visual Component Library (VCL). Dynamic visualisation of results is possible using the TChart component, with customisable axis parameters and data series.

The programmes have implemented loading and processing data from text files and a database. They consist of several logically separated modules: user interface, data loading and processing module and a visualisation module.

The test of both applications was carried out during the operation of the laboratory bench on 13.03.2025. The measurements were carried out so that the steam header is taken out of circulation during the start-up of the steam boiler and steam generation. Once the steam pressure and temperature were sufficiently high, the valve upstream of the steam header was opened. The experiment carried out in this way made it possible to obtain an unsteady temperature field in the steam header. During the start-up of the stand, the manometric pressure in the header increased to 300 kPa, the mass flux of steam flowing through the header after opening the valve was about 450 kg/h, then was reduced to about 300 kg/h. The steam temperature was approximately 140°C.

Both applications were run while the laboratory bench was in operation, and calculations were performed online. The interface windows of both applications are shown in Figs. 9−10, which are screenshots of the computer operating the bench. The user interface was designed in both cases so that the central part consists of two graphs, where the upper one presents the measurement data and the lower one presents the calculation results. The graphs present data for the last 500 s. Next to the graphs, on the right-hand side, there is a legend describing the curves drawn. A detailed data description appears when the cursor is placed on the chart area or the legend. The user can also select which data they wish to present on the graphs by ticking the appropriate check boxes in the legend. On the right side of the programme window, there is a visualisation of the location of temperature measurement points in the steam header wall and information on the funder, i.e. the National Science Centre in Poland, whose funding allowed the research to be carried out.

The 'Thermal Stress Monitoring' application window is shown in Fig. 9. In Fig. 9, the top graph shows the measured data, i.e. the temperature at point N (labelled *T*_N), the temperature of the steam measured by sheathed thermocouples with diameters of 1 mm, 2 mm and 3 mm (*T_f* ϕ 1 mm, *T_f* ϕ 2 mm, and *T_f* ϕ 3 mm, respectively), the pressure of the steam flowing through the steam header *p* and the mass flux of the steam *m*. The temperature measuring point N in the wall of the steam collector is located at 7.5 mm from the inner surface. The bottom graph shows the calculated data, i.e.: the stress on the inner surface caused by the pressure σ_*p*, the thermal stress on the inner surface σ_*T*, the sum of both stresses $\sum\sigma$, the temperature of the inner surface *T_in*, the temperature of the outer surface *T_out* and the difference of these temperatures, i.e. *T_out* − *T_in*. The temperatures *T_in* and *T_out* are also summarised in the top graph to make comparing them with the measured temperatures easier.

The thermal stresses on the inner surface of the header are highest during the temperature step change in the header and reach a maximum value of −195.8 MPa. In turn, the stresses caused by pressure are minimal due to the low steam pressures, reaching a maximum of 0.9 MPa for the highest pressure value of 300.1 kPa obtained towards the end of the experiment. Consequently, the σ_*T* and $\sum\sigma$ curves coincide.

In turn, Fig. 10 shows the application window 'Identification of Heat Transfer Coefficient'. The top graph shows the temperature measurements carried out at six points: C, N, W, S, E and

U (corresponding to the designations *T*_C, *T*_N, *T*_W, *T*_S, *T*_E and *T*_U, respectively). Points C, N, W, S and E are located at a distance of 7.5 mm from the inner surface, where N, W, S and E are spaced 50 mm from the central point of C, N and S are respectively above and below point C in the circumferential direction, and E and W are located to the right and left of point C in the longitudinal direction. Point U is located 15 mm from the inner surface and 7.5 mm from centre point C in the radial direction.

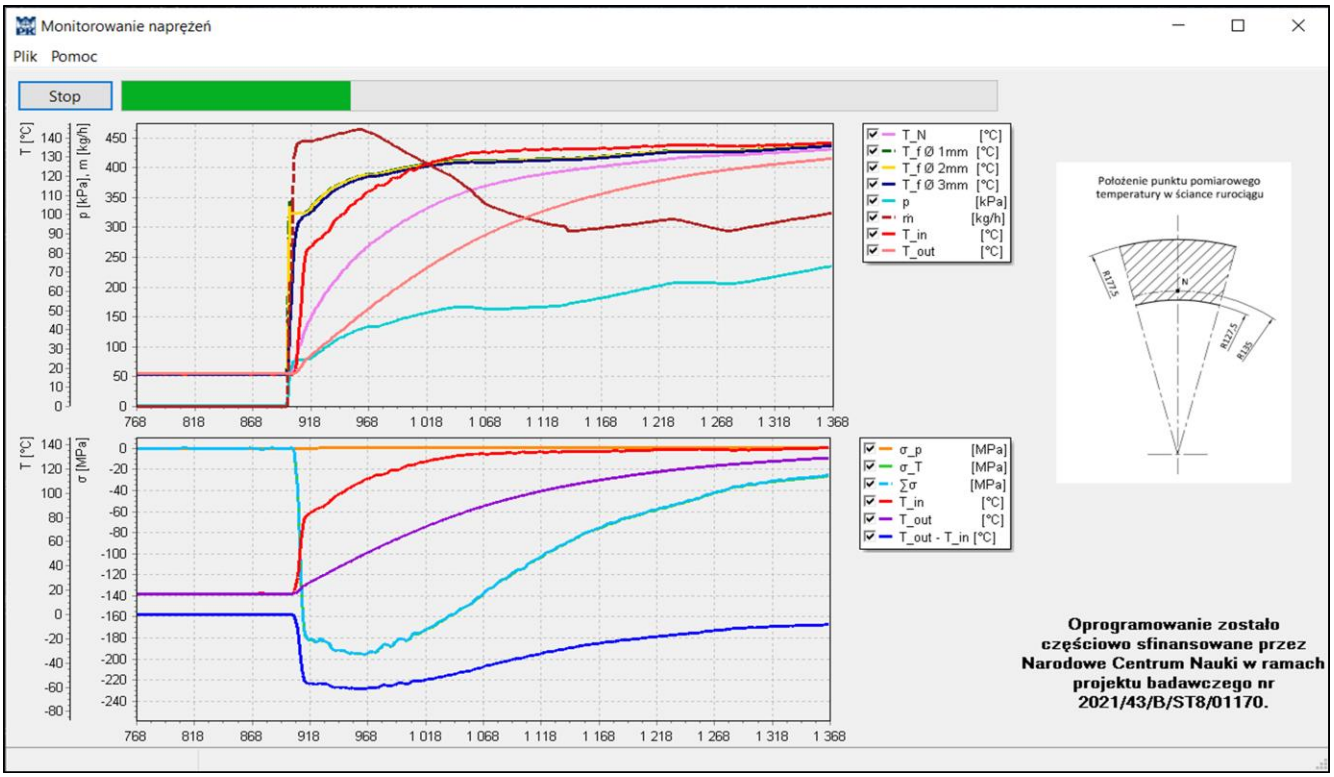

Fig. 9. Screenshot of the 'Thermal Stress Monitoring' application window during operation of the installation on 13.03.2025.

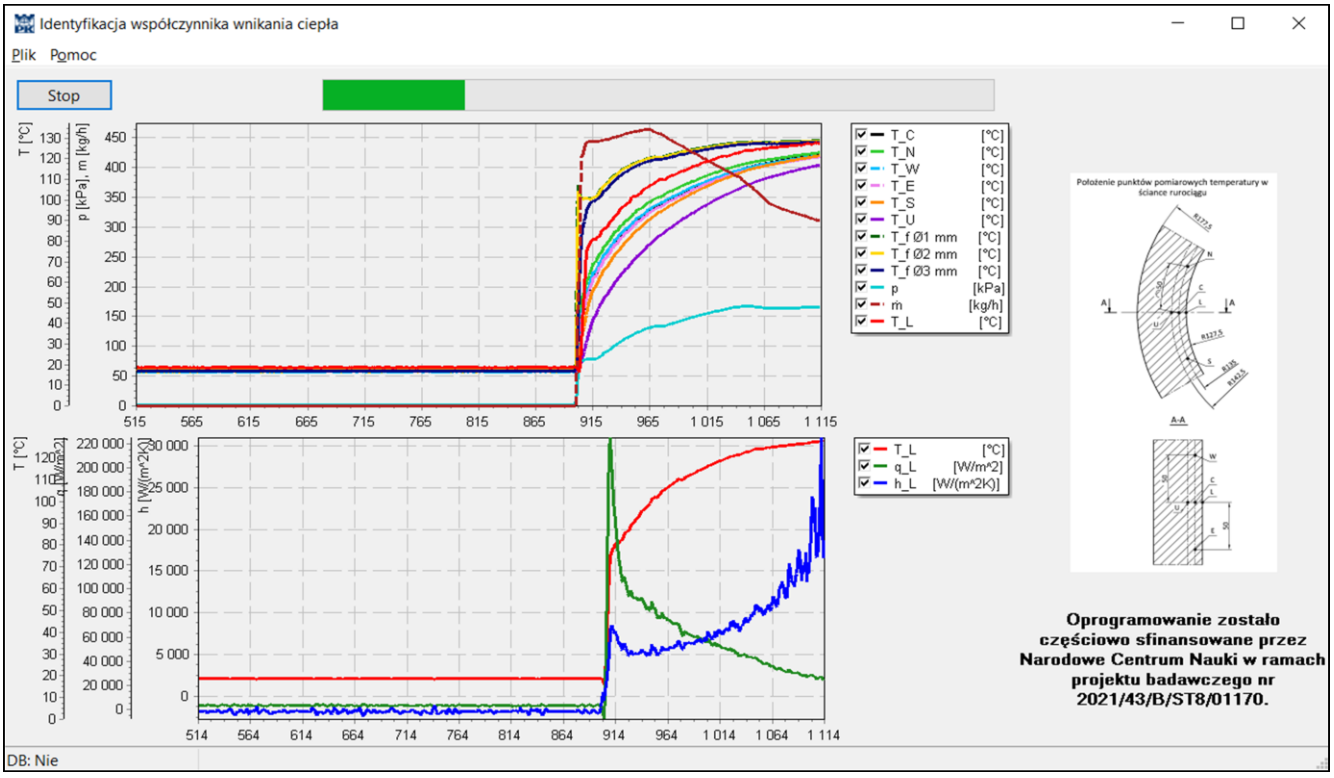

Fig. 10. Screenshot of the 'Identification of Heat Transfer Coefficient' application window during operation of the installation on 13.03.2025.

In addition, the upper graph presents the steam temperature measurements with 1 mm, 2 mm and 3 mm diameter thermometers ($T_f\,\phi$1 mm, $T_f\,\phi$2 mm, and $T_f\,\phi$3 mm), the pressure in the header (p) and the mass flux of steam (m). The bottom graph presents the results of the calculations, i.e. the temperature (T_L), the heat flux (q_L) and the heat transfer coefficient (h_L) at point L on the internal surface. Point L lies in the same radial direction as points U and C. The highest value of heat flux is 224 537.5 W/m^2 and is achieved during the opening of the valve at the inlet to the steam header and during the first moments of steam flow, when the temperature difference between the inner surface of the pipe and the working fluid is greatest. The heat transfer coefficient is then 7897.5 W/(m^2 K). Thereafter, the heat flux value begins to decrease. The heat transfer coefficient decreases with the heat flux for the first 30 seconds, then remains at approximately 5000 W/(m^2 K) for approximately 1 minute. After that, the smaller the difference between the surface temperature and steam temperature and the heat flux, the higher the heat transfer coefficient.

The impact of sensor measurement uncertainty on the accuracy of calculations was negligible. Temperature measurements were used in the calculations of thermal stresses and the heat transfer coefficient. Thanks to the calibration of the measuring sensors in a calibration furnace prior to their installation, the impact of temperature measurement uncertainty on the calculation results is insignificant. In addition, pressure gauge measurements were used to calculate the stresses caused by pressure. Since their value is small compared to thermal stresses, the uncertainty of pressure measurement is of little significance.

Both programmes generate reports with calculation data in a text file (.txt).

6. Conclusions

The article presents calculation algorithms that allow determining circumferential stresses and the heat transfer coefficient on the inner surface of a thick-walled cylindrical element. The algorithm for determining thermal stresses can be used for one-dimensional heat conduction (in the radial direction) and is based on measuring the wall temperature at a single point. The algorithm for determining the heat transfer coefficient is suitable for heat conduction in a thick-walled element in three directions: radial, circumferential and longitudinal. It is based on measuring the wall temperature at six points – a special measuring probe was made for this purpose. The solution to the inverse heat conduction problem was used in both cases.

Based on the described algorithms, two applications were created that can be used online, which is particularly important in unsteady states. The applications have been tested on a test bench and are functioning correctly. The calculations were made on the basis of measurements taken in a thick-walled steam header that is part of a large system with a steam boiler. The experiment was conducted by suddenly opening the valve upstream of the header, allowing steam to flow through it. The temperature in the header rapidly rose from 16.8°C to 142.5°C. At the beginning of the sudden temperature change, the thermal stresses on the inner surface of the pipe reached a maximum value of −195.8 MPa, and the heat transfer coefficient reached a value of approximately 5000 W/(m² K). Subsequently, as the collector wall temperature stabilised, a decrease in thermal stresses and an increase in the heat transfer coefficient occurred.

The applications can be an effective tool for monitoring thermal stresses in pressure components.

Acknowledgements

This work was supported by the National Science Centre in Poland under Grant No. 2021/43/B/ST8/01170.

References

[1] Chen, M., Qiu, H. & Li, F. (2023). Monitoring of thermal stress in metal plates by using bonded shear horizontal wave piezoelectric transducers. *Ultrasonics*, 129, 106905. doi: 10.1016/j.ultras.2022.106905

[2] Taler, D., Dzierwa, P., Kaczmarski, K., & Taler, J. (2022). Increase the flexibility of steam boilers by optimisation of critical pressure component heating. *Energy*, 250. doi: 10.1016/j.energy.2022.123855

[3] Taler, D., Kaczmarski, K., Dzierwa, P., Taler, J. & Trojan, M. (2024). Optimisation of the cooling of pressurised thick-walled components operating with fluid at saturation temperature. *Energy*, 290, 129975. doi: 10.1016/j.energy.2023.129975

[4] TRD 301 (2001). *Zylinderschalen unter innerem Überdruck. Technische Regeln für Dampfkessel* (TRD), Heymanns Beuth Köln-Berlin.

[5] European Standard EN 12952-3 (2001). *Water-tube boilers and auxiliary installations. Part 3: design and calculation for pressure parts.* European Committee for Standardization.

[6] Banaszkiewicz, M. (2021). Concept of advanced lifetime monitoring system for steam turbines. *Diagnostyka*, 22(1), 23−29. doi: 10.29354/diag/132548

[7] Rusin, A., Tomala, M., Łukowicz, H., Nowak, G., & Kosman, W. (2021). On-Line Control of Stresses in the Power Unit Pressure Elements Taking Account of Variable Heat Transfer Conditions. *Energies*, 14(15), 4708. doi: 10.3390/en14154708

[8] Radin, Y.A., Kontorovich, T.S., & Golov, P.V. (2020). Monitoring the Thermal Stress State in Steam Turbines. *Power Technology and Engineering*, 53(6), 719–723. doi: 10.1007/s10749-020-01146-6

[9] Radin, Y.A., & Kontorovich, T.S. (2021). Influence of the Arrangement of the Highand Intermediate-Pressure Cylinders of Steam Turbines with Different Bypass Circuits on their Thermal Stress State During Start-Ups and Shutdowns. *Power Technology and Engineering*, 54(5), 720–725. doi: 10.1007/s10749-020-01276-x

[10] Radin, Y.A., & Kontorovich, T.S. (2024). Influence of Parameter Deviations Vis-a-Vis Assignment Schedule on Thermally Stressed State of Main Thermal Power Plant Equipment. *Power Technology and Engineering*, 57(6), 918–921. doi: 10.1007/s10749-024-01758-2

[11] Oliver, S., Simpson, C., Collins, D.M., Reinhard, C., Pavier, M. & Mostafavi, M. (2021). In-situ measurements of stress during thermal shock in clad pressure vessel steel using synchrotron X-ray diffraction. *International Journal of Mechanical Sciences*, 192, 106136. doi: 10.1016/j.ijmecsci.2020.106136

[12] Oh, C., Lee, S., Jhung, M.J., & Huh N.-S. (2022). Analytical approach to estimate the thermal stress distribution of reactor pressure vessel nozzle corners with a constant cooldown rate. *International Journal of Pressure Vessels and Piping*, 197, 104608. doi: 10.1016/j.ijpvp.2022.104608

[13] Jeong, S.-H., Chung, K.-S., Ma, W.-J., Yang, J.-S., Choi, J.-B., & Kim, M. K. (2022). Thermal stress intensity factor solutions for reactor pressure vessel nozzles. *Nuclear Engineering and Technology*, 54, 2188–2197. doi: 10.1016/j.net.2022.01.006

[14] Pernica, M., Létal, T., Lošák, P., Naď, M., Reppich, M. & Jegla, Z. (2021). Transient Thermal Stress Calculation of a Shell and Tube Condenser with Fixed Tubesheet. *Chemie Ingenieur Technik*, 93 (10), 1590−1597. doi: 10.1002/cite.202100036

[15] Okrajni, J., Twardawa, M., & Wacławiak, K. (2021). Impact of Heat Transfer on Transient Stress Fields in Power Plant Boiler Components. *Energies*, 14(4), 862. doi: 10.3390/en14040862

[16] Teixeira Júnior, M., Zilio, G., Mortean, M.V.V., de Paiva, K.V., & Oliveira, J.L.G. (2023). Experimental and numerical analysis of transient thermal stresses on thick-walled cylinder. *International Journal of Pressure Vessels and Piping*, 202, 104884. doi: 10.1016/j.ijpvp.2023.104884

[17] Jaremkiewicz, M., Dzierwa, P., Taler, D., & Taler, J. (2019). Monitoring of transient thermal stresses in pressure components of steam boilers using an innovative technique for measuring the fluid temperature. *Energy*, 175, 139-150. doi: 10.1016/j.energy.2019.03.049

[18] Taler, J., & Duda, P. (2000). Experimental verification of space marching methods for solving inverse heat conduction problems. *Heat and Mass Transfer*, 36, 325–331. doi: 10.1007/s002310000082

[19] Taler, J., Zima, W., & Jaremkiewicz, M. (2016). Simple method for monitoring transient thermal stresses in pipelines. *Journal of Thermal Stresses*, 39, 386–397. doi: 10.1080/01495739.2016.1152109

[20] Jaremkiewicz, M. & Taler, J. (2017). Measurement of Transient Fluid Temperature in a Pipeline. *Heat Transfer Engineering*, 39(13–14), 1227–1234. doi: 10.1080/01457632.2017.1363631.

[21] Taler, D., Taler, J., Kaczmarski, K., Jaremkiewicz, M., Dzierwa, P. & Trojan, M. (2024). Monitoring of thick-walled pressure elements to determine transient temperature and stress distributions using the measured fluid's pressure and wall's temperature. *Energy*, 309, 133121. doi: 10.1016/j.energy.2024.133121

[22] Taler, J., Kaczmarski, K., Taler, D., Dzierwa, P., Trojan, M., & Sobota, T. (2025). Online determination of the heat transfer coefficient at the inner surface of a cylindrical component in a thermal stress monitoring system for critical boiler pressure components. *Energy*, 328. doi:10.1016/j.energy.2025.136637

[23] Kushnir, R.M., Yasinskyy, A.V. & Tokovyy, Y.V. (2022). Effect of Material Properties in the Direct and Inverse Thermomechanical Analyses of Multilayer Functionally Graded Solids. *Advanced Engineering Materials*, 24, 2100875, 1−10. doi: 10.1002/adem.202100875

[24] Ciałkowski, M., Joachimiak, M., Mierzwiczak, M., Frąckowiak, A., Olejnik, A. & Kozakiewicz, A. (2023). The analysis of the stability of the Cauchy problem in the cylindrical double-layer area. *Archives of Thermodynamics*, 44(4), 563–579. doi: 10.24425/ather.2023.149735

[25] Joachimiak, M. & Joachimiak, D. (2024). Stabilization of boundary conditions obtained from the solution of the inverse problem during the cooling process in a furnace for thermo-chemical treatment. *International Journal Heat and Mass Transfer*, 224, 125274. doi: 10.1016/j.ijheatmasstransfer.2024.125274

[26] Joachimiak, M., Joachimiak, D. & Ciałkowski, M. (2022). Investigation on Thermal Loads in Steady-State Conditions with the Use of the Solution to the Inverse Problem. *Heat Transfer Engineering*, 44(11–12), 963–969. doi: 10.1080/01457632.2022.2113451

[27] Taler, J.(1999). A new space marching method for solving inverse heat conduction problems. *Forschung im Ingenieurwesen*, 64, 296–306. doi: 10.1007/PL00010844

[28] Taler, J., & Duda, P. (2006). *Solving Direct and Inverse Heat Conduction Problems*. Springer.

[29] Taler, J. (1995). *Theory and practice of identifying heat transfer processes*. Zakład Narodowy im. Ossolińskich (in Polish).